Computer Physics Communications 252 (2020) 107131

Contents lists available at ScienceDirect

Computer Physics Communications

journal homepage: www.elsevier.com/locate/cpc

Full 3D position reconstruction of a radioactive source based on a novel hyperbolic geometrical algorithm☆

Costanza M.V. Panaino [a,*], Ranald I. Mackay [a,b], Marios Sotiropoulos [a], Karen J. Kirkby [a,b], Michael J. Taylor [a,b]

[a] Division of Cancer Sciences, University of Manchester, M13 9PL, Manchester, UK
[b] The Christie NHS Foundation Trust, M20 4BX, Manchester, UK

ARTICLE INFO

Article history:
Received 30 May 2019
Received in revised form 2 December 2019
Accepted 16 December 2019
Available online 26 December 2019

Keywords:
Reconstruction algorithm
Gamma-ray spectroscopy
Source emission position reconstruction

ABSTRACT

A new method to locate, with millimetre uncertainty, in 3D, a γ-ray source emitting multiple γ-rays in a cascade, employing conventional $LaBr_3$(Ce) scintillation detectors, has been developed. Using 16 detectors in a symmetrical configuration the detector energy and time signals, resulting from the γ-ray interactions, are fed into a new source position reconstruction algorithm. The Monte-Carlo based Geant4 framework has been used to simulate the detector array and a ^{60}Co source located at two positions within the spectrometer central volume. For a source located at (0,0,0) the algorithm reports X, Y, Z values of -0.3 ± 2.5, -0.4 ± 2.4, and -0.6 ± 2.5 mm, respectively. For a source located at (20,20,20) mm, with respect to the array centre, the algorithm reports X, Y, Z values of 20.2 ± 1.0, 20.2 ± 0.9, and 20.1 ± 1.2 mm. The resulting precision of the reconstruction means that this technique could find application in a number of areas including nuclear medicine, national security, radioactive waste assay and proton beam therapy.

© 2019 The Author(s). Published by Elsevier B.V. This is an open access article under the CC BY-NC-ND license (http://creativecommons.org/licenses/by-nc-nd/4.0/).

1. Introduction

There are a number of instances where the knowledge of the location of a source of radiation is highly desirable. One example is in cargo scanning where the detection and localisation of illegal radioactive sources could be a major concern for national security. The need to accurately locate radioactive samples is also a crucial requirement in the nuclear energy industry. Radioactive waste measurement instruments, for instance, employ various technologies to locate and quantify the radioactive content in waste samples [1]. In nuclear medicine the position reconstruction of an emitting source represents the core of emission tomographic imaging techniques, such as Single Photon Emission Computed Tomography (SPECT) [2].

The ability to determine the location of a γ-rays source, with high precision using conventional radiation detectors, is a challenge. Some existing techniques utilise the Time Of Flight (TOF) of γ-rays, where both the start (i.e. emission) time and the final (i.e. detection) time of the rays is needed. Usually the final time is provided by the radiation detection instrument but the start time can be extremely difficult to obtain, in particular for radioactive sources.

For distributed sources, such as those produced during Proton Beam Therapy (PBT) in cancer treatment, the challenge can be even greater. The precise knowledge of the beam range is essential to guarantee the treatment's efficacy and to avoid toxicities. One proposed method to assess *on-line* proton range verification is given by the detection of the Prompt-Gamma (PG) rays naturally produced during therapy [3]. After an inelastic interaction with an incoming proton the target nucleus is excited to higher energy states and, to return to its ground state, it emits γ-rays [4]. These emissions are almost instantaneous [5] (hence the use of the adjective *prompt*), high in energy (2–15 MeV) [6] and are characterised by a high production rate [7]. A good correlation between the beam range and the intensity of the PG-rays emitted by the most abundant isotopes in human tissues, namely C, O and N, has been experimentally proven [7]. The reconstruction of the PG-rays emitting positions inside the patients' bodies may allow to precisely check the actual location of the proton beams during radiotherapy.

In this work a new method to determine the location of a source of γ-ray radiation with millimetric accuracy for both localised and distributed sources has been developed. The method uses only the signals from conventional, non-position sensitive, fast-timing scintillation detectors. For proof-of-principle $LaBr_3$ (Ce) detectors, arranged in a symmetrical configuration, have been employed to feed into a novel source position reconstruction algorithm that determines the source origin.

☆ The review of this paper was arranged by Prof. Z. Was.

* Corresponding author.
E-mail address: costanza.panaino@postgrad.manchester.ac.uk (C.M.V. Panaino).

https://doi.org/10.1016/j.cpc.2019.107131
0010-4655/© 2019 The Author(s). Published by Elsevier B.V. This is an open access article under the CC BY-NC-ND license (http://creativecommons.org/licenses/by-nc-nd/4.0/).

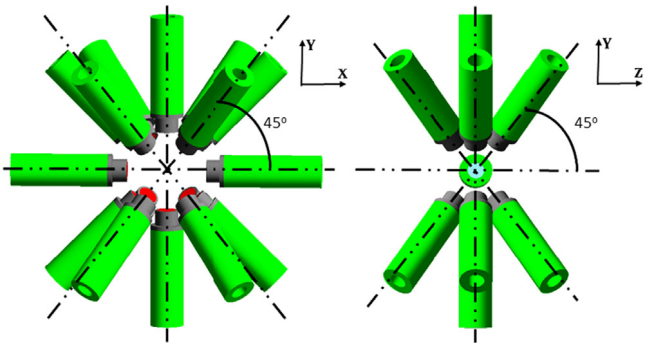

Fig. 1. The spectrometer utilised in this work for source position reconstruction is composed of sixteen $LaBr_3$(Ce) scintillation detectors arranged in a symmetrical configuration.

2. Methods

2.1. Source reconstruction method

The technique developed in this work utilises the coincident detection of the γ-rays emitted in a cascade by a radioactive source or following inelastic nuclear reactions. The emission time difference between these γ rays, if the intermediate state is not isomeric, is on the order of pico or femto seconds, which is short compared to the time resolution of a typical scintillator detector ($\sim$ 400–500 ps [8]). Within this limitation of current detector and electronic systems, the two γ de-excitations are effectively emitted simultaneously in time and position. The detection of a *couple* of γ-rays in coincidence, together with a reconstruction algorithm, may allow the identification of the common emission point. As a proof-of-principle a ^{60}Co isotropic point source can be employed. The ^{60}Co decay scheme consists of two γ-rays of 1.173 and 1.332 MeV emitted in a cascade. The adopted value for the intermediate state lifetime is 0.713 ps [9].

2.2. γ-ray Spectrometer

In SPECT, source position determination is only possible through the mechanical collimation of the radiation detector. This minimises the available signal and therefore limits the technique to sources of a particular intensity [10]. The technique developed in this work does not require any collimation of the radiation detectors. Fig. 1 shows diagrammatically the proof-of-principle spectrometer used which is composed of 16 $LaBr_3$(Ce) cylindrical detectors with dimensions 2″ length and 1.5″ diameter. The detectors are arranged as follows: a ring of eight symmetrically-spaced detectors in the vertical plane plus one ring of four detectors at backward angles (45°) and one ring of four detectors at forward angles (45°), with respect to the Z axis. For an isotropic source in the centre of the spectrometer, when the distance between the source and the front face of all detectors is 9 cm, this geometry covers 24% of the total solid angle. The energy resolution of $LaBr_3$(Ce), $\sim$ 40 keV Full Width at Half Maximum (FWHM) at 1.33 MeV, makes it a suitable detector for high energy γ-ray spectroscopy. In addition the intrinsic time resolution of $LaBr_3$(Ce) detectors is sub-nanosecond from a few keV up to 4 MeV, giving excellent time discrimination [11]. $LaBr_3$(Ce) crystals possess internal activity, predominantly due to the decay of ^{138}La. The γ-rays arising from this activity do not interfere with the source γ-rays due to the coincidence requirement of the algorithm.

2.3. Position reconstruction algorithm

A source position reconstruction algorithm has been developed within the MATLAB environment (version R2017b). For every γ-ray γ_i recorded by the spectrometer several pieces of information are saved and passed to the algorithm; the energy E_i, the time t_i and the detector number Det_i. The algorithm takes as input the detector signals from two correlated γ-rays and determines their common emission position. In order to reconstruct the emission position, the data goes through three main functions: (1) γ-Ray *Couple* Selection, (2) γ-Ray *Couple* Analysis, and (3) γ-Ray *Couple* Emission-Position Reconstruction. A flowchart detailing the algorithm is shown in Fig. 2 and described in Sections 2.3.1, 2.3.2, 2.3.3, and 2.3.4.

2.3.1. Function 1: γ-ray couple selection

The algorithm selects *couples* of γ-rays, γ_i and γ_{i+1}, which satisfy the following criteria:

1. The two events, γ_i and γ_{i+1}, were recorded in coincidence in two different detectors, i.e. $Det_i \neq Det_{i+1}$.
2. The energies E_i and E_{i+1} of the two events are 1.173 and 1.332 MeV, irrespective of order.

At 1.332 MeV the $LaBr_3$(Ce) energy resolution is 3% FWHM [12] (Full Width Half Maximum). In this case the algorithm accepts γ-ray energies of 1.173 and 1.332 MeV $\pm$ 3%. At the end of this function only those events which belong to a γ-ray *couple* are saved. Those events which do not fulfil the criteria above are rejected.

For radioactive sources the γ-ray emission time is not usually measurable, however, using a coincidence technique the time difference ($\Delta t = | t_{i+1} - t_i |$) between two consecutive events (γ_i and γ_{i+1}, with γ_{i+1} being detected after γ_i) can be obtained. The algorithm has been designed to utilise, for each correlated *couple* of γ-rays, the time difference (Δt).

2.3.2. Function 2: γ-ray couple analysis

An hyperbola is a conic section defined as the locus of points P such that the difference of the distance from P to two fixed points, F_1 and F_2, called foci, is a constant value k [13]. A two-sheeted hyperboloid is a quadratic surface obtained by rotating an hyperbola about the line joining the foci [13]. For each *couple* a two-sheeted hyperboloid is constructed. The foci correspond to the hit coordinates of the two events. The constant distance k is the absolute value of the time difference between the two events Δt multiplied by the speed of light c. The source position should lie somewhere on the hyperboloid surface. For example, as shown schematically in Fig. 3 and in 3D in Fig. 4, for a source located in (x_s, y_s, z_s), the events γ_i and γ_{i+1}, detected in (x_i, y_i, z_i) and $(x_{i+1}, y_{i+1}, z_{i+1})$, at time t_i and t_{i+1} respectively, are represented by a two-sheeted hyperboloid having foci in (x_i, y_i, z_i) and in $(x_{i+1}, y_{i+1}, z_{i+1})$ and constant k value $\Delta t \cdot c = |t_{i+1} - t_i| \cdot c$. In other words the two-sheeted hyperboloid can be defined as the locus of points that satisfy the following Equation:

$$\sqrt{(x-x_i)^2+(y-y_i)^2+(z-z_i)^2} - \sqrt{(x-x_{i+1})^2+(y-y_{i+1})^2+(z-z_{i+1})^2} = \pm \Delta t \cdot c \quad (1)$$

where $(x_s, y_s, z_s) \in (x, y, z)$.

The $\pm$ sign on the right hand side of Eq. (1) defines the two sheets of the hyperboloid.

- If $t_{i+1} - t_i > 0$:

$$\sqrt{(x-x_i)^2+(y-y_i)^2+(z-z_i)^2} - \sqrt{(x-x_{i+1})^2+(y-y_{i+1})^2+(z-z_{i+1})^2} = - \Delta t \cdot c \quad (2)$$

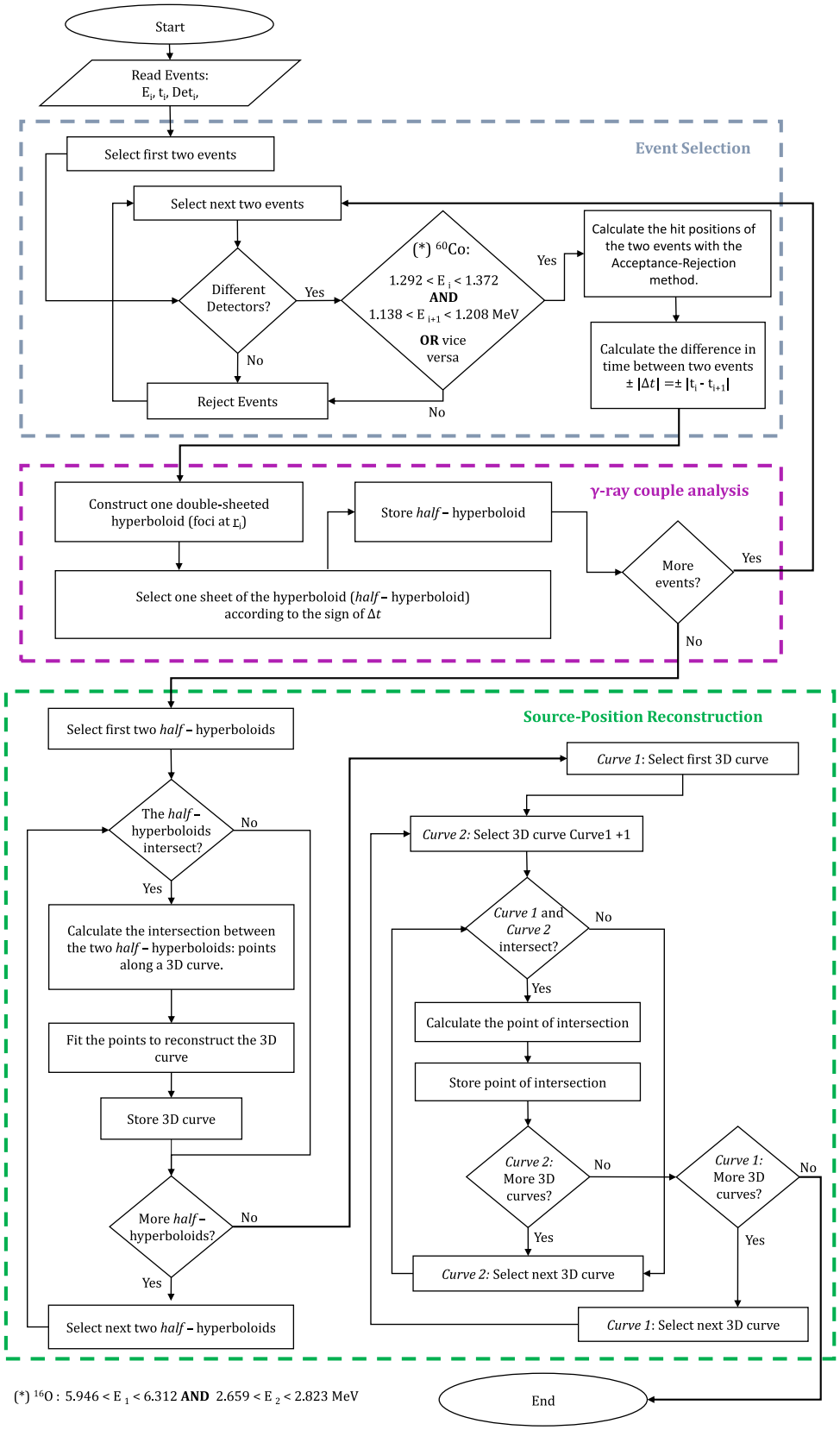

Fig. 2. Flowchart of the 3D reconstruction algorithm developed in the MATLAB framework. To reconstruct the source position a sequence of steps is undertaken. These steps are represented by three main functions: (1) γ-Ray *Couple* Selection, (2) γ-Ray *Couple* Analysis, and (3) Source-Position Reconstruction. The algorithm has been specifically optimised to utilise those input data, from Geant4 simulations, that are available in real γ-spectroscopy experiments.

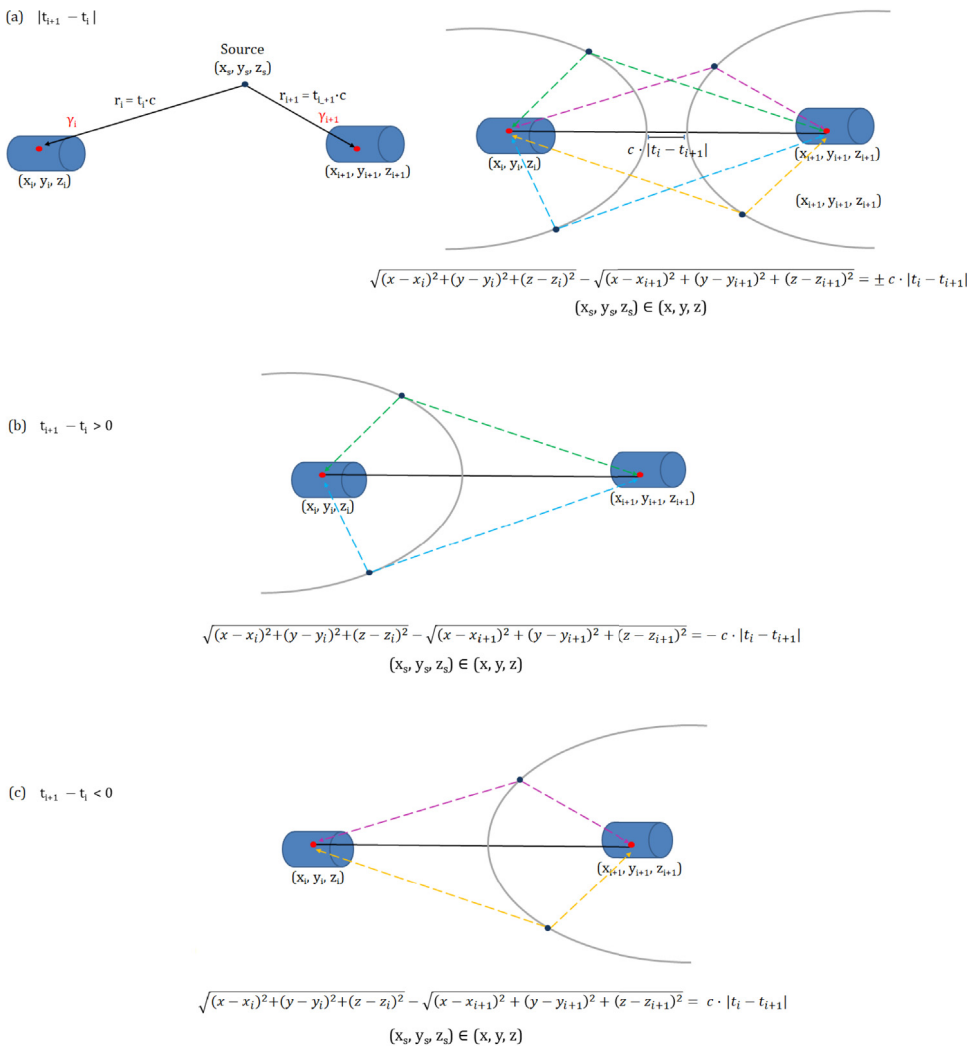

Fig. 3. (a) Schematic illustration of the second function of the algorithm, γ-Ray *Couple* Analysis: for each *couple* of γ-rays, γ_i and γ_{i+1}, a two-sheeted hyperboloid is constructed. The hit coordinates (x_i, y_i, z_i) and $(x_{i+1}, y_{i+1}, z_{i+1})$ represent the foci. The difference between the distance each point of the hyperboloid has with the two foci is a constant value k. To estimate k the absolute value of the time difference between γ_i and γ_{i+1}, $\Delta t = |t_{i+1} - t_i|$, is employed. (b) – (c) If the sign of Δt is known each *couple* is represented by a sheet only of the two-sheeted hyperboloid (named *half*-hyperboloid).

- If $t_{i+1} - t_i < 0$:

$$\sqrt{(x-x_i)^2+(y-y_i)^2+(z-z_i)^2} - \sqrt{(x-x_{i+1})^2+(y-y_{i+1})^2+(z-z_{i+1})^2} = + \Delta t \cdot c \quad (3)$$

If the sign of Δt is known, Eq. (1) can be reduced to Eq. (2) or to Eq. (3). In other worlds a *couple* is associated with only one side of a two-sheeted hyperboloid (here named *half*-hyperboloid). It is possible to reduce Eq. (1) to Eqs. (2) or (3) even if the sign of Δt is not known. This can be achieved through an analysis of the intensity recorded by each detector unit. A high intensity implies a higher subtended solid angle, relative to the source position and a shorter relative arrival time, both due to a shorter γ-ray path length.

Given two events in a *couple* γ_i and γ_{i+1}, detected in Det_i and Det_{i+1}, the following assumptions can be made:

- if $Tot_{events_j}|_{j=Det_i} < Tot_{events_j}|_{j=Det_{i+1}} \rightarrow t_i > t_{i+1}$ Eq. (1) can be reduced to Eq. (2).
- if $Tot_{events_j}|_{j=Det_i} > Tot_{events_j}|_{j=Det_{i+1}} \rightarrow t_i < t_{i+1}$ Eq. (1) can be reduced to Eq. (3).

where $Tot_{events_j}|_{j=Det_i}$ is the total number of γ-rays belonging to *couples* and recorded in Det_i.

It is desirable that every time the condition $Tot_{events_j}|_{j=Det_i} < Tot_{events_j}|_{j=Det_{i+1}}$ is satisfied the condition $t_i > t_{i+1}$ is also true, and vice versa.

2.3.3. Function3: Source position reconstruction — intersection between half-hyperboloids

At the end of the previous function n *half*-hyperboloids are stored. In the third function of the algorithm each couple of subsequent *half*-hyperboloids (1/2, 3/4, …, $n/(n+1)$, …) is retrieved and, as illustrated in Fig. 5, their intersection is determined. The maximum number of intersections, $n/2$, is achieved when all of the *half*-hyperboloids couples intersect. The intersections are obtained by triangulating the surfaces of two subsequent *half*-hyperboloids. A triangulated *half*-hyperboloid is a *half*-hyperboloid whose surface has been totally divided into a net of triangles in such a way that every internal point belongs to a triangle, and the intersection of any two triangles is either void, a common side or a common vertex [14].

Each intersection between two subsequent hyperboloids is then parameterised by a series of points in 3D space following a single trajectory.

As shown in Fig. 6a each intersection between two *half*-hyperboloids is calculated in a virtual voxelised cube located

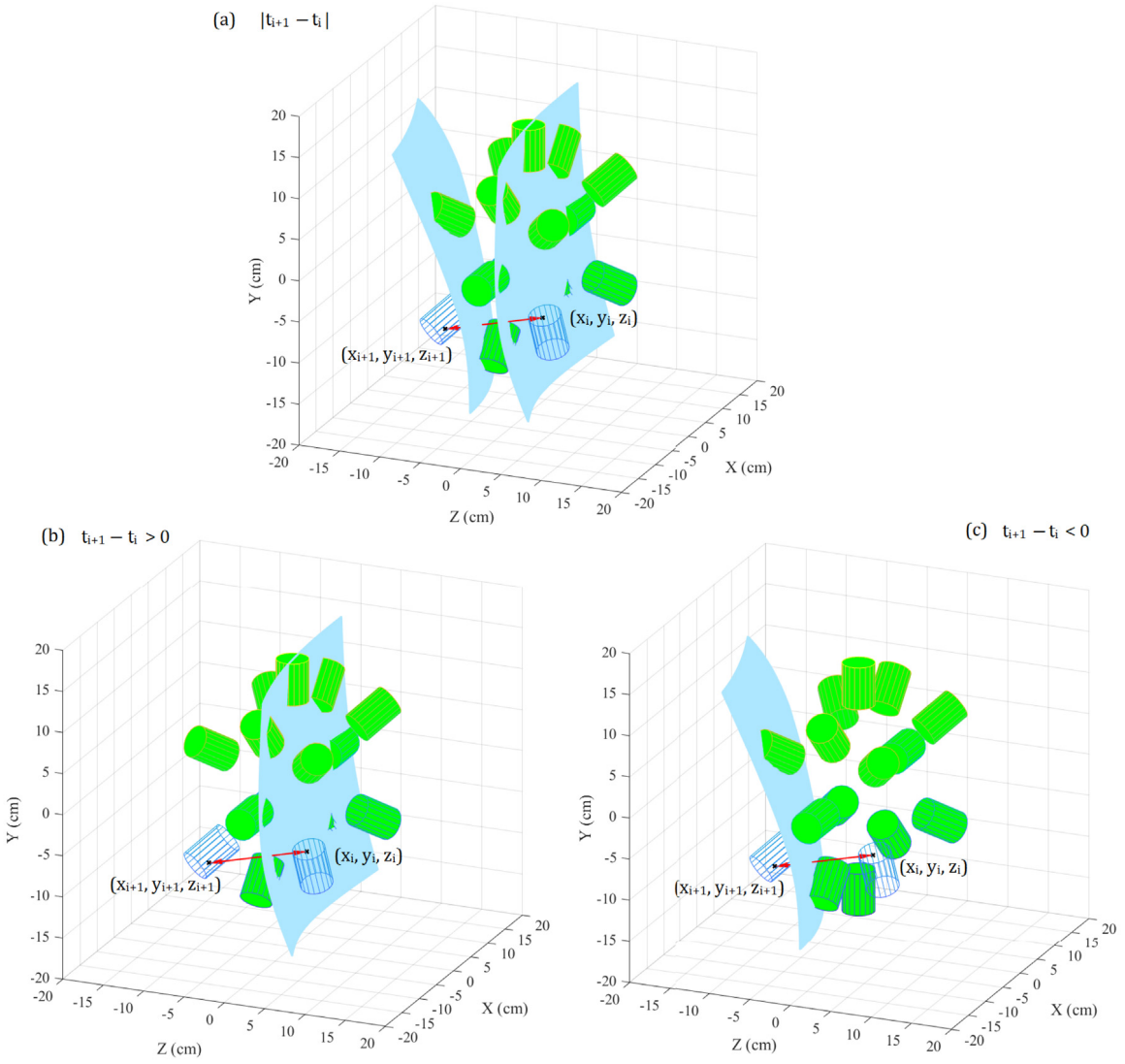

Fig. 4. (a) 3D illustration of the second function of the algorithm, γ-Ray *Couple* Analysis: for each *couple* of γ-rays γ_i and γ_{i+1} a two-sheeted hyperboloid is constructed where the hit coordinates (x_i, y_i, z_i) and (x_{i+1}, y_{i+1}, z_{i+1}) are the foci. (b) – (c) If the sign of Δt is known each *couple* is represented by a sheet only of the two-sheeted hyperboloid (named *half*-hyperboloid).

in the central area of the spectrometer. The larger the dimensions of this cube (X_{neg}/X_{pos}, Y_{neg}/Y_{pos}, Z_{neg}/Z_{pos}) the wider the sampled area. If two *half*-hyperboloids intersect at a specific voxel the central point of that voxel is saved as an intersection point. Consequently the smaller the voxel size v_{dim}, for a constant sample area, the more intersection points may be produced. By both increasing the cube size and/or decreasing the voxels size the algorithm computational time extends. To reduce the cube size, along the three axes independently, the intensity of the γ-rays recorded in the detectors at backward/forward angles ($Tot_{events_j}|_{j=Det_9-Det_{16}}$) can be employed. In this regard, with reference to Fig. 6b, the following analysis is performed:

- To check if the source X coordinate is positive or negative
  1. $X = [0, X_{pos}]$ if:
     $\sum_{j=Det_{10},Det_{11},Det_{13},Det_{15}} \sum_{i=Det_9,Det_{12},Det_{14},Det_{16}} \left(Tot_{events_j} - \sqrt{Tot_{events_j}}\right) > \left(Tot_{events_i} - \sqrt{Tot_{events_i}}\right)$
  2. $X = [X_{neg}, 0]$ if:
     $\sum_{j=Det_{10},Det_{11},Det_{13},Det_{15}} \sum_{i=Det_9,Det_{12},Det_{14},Det_{16}} \left(Tot_{events_j} - \sqrt{Tot_{events_j}}\right) > \left(Tot_{events_i} - \sqrt{Tot_{events_i}}\right)$
- To check if the source Y coordinate is positive or negative
  1. $Y = [0, Y_{pos}]$ if:
     $\sum_{j=Det_9,Det_{10},Det_{15},Det_{16}} \sum_{i=Det_{11},Det_{12},Det_{13},Det_{14}} \left(Tot_{events_j} - \sqrt{Tot_{events_j}}\right) > \left(Tot_{events_i} - \sqrt{Tot_{events_i}}\right)$
  2. $Y = [Y_{neg}, 0]$ if:
     $\sum_{j=Det_9,Det_{10},Det_{15},Det_{16}} \sum_{i=Det_{11},Det_{12},Det_{13},Det_{14}} \left(Tot_{events_j} - \sqrt{Tot_{events_j}}\right) > \left(Tot_{events_i} - \sqrt{Tot_{events_i}}\right)$
- To check if the source Z coordinate is positive or negative
  1. $Z = [0, Z_{pos}]$ if:
     $\sum_{j=Det_9,Det_{10},Det_{11},Det_{12}} \sum_{i=Det_{13},Det_{14},Det_{15},Det_{16}} \left(Tot_{events_j} - \sqrt{Tot_{events_j}}\right) > \left(Tot_{events_i} - \sqrt{Tot_{events_i}}\right)$
  2. $Z = [Z_{neg}, 0]$ if:
     $\sum_{j=Det_9,Det_{10},Det_{11},Det_{12}} \sum_{i=Det_{13},Det_{14},Det_{15},Det_{16}} \left(Tot_{events_j} - \sqrt{Tot_{events_j}}\right) > \left(Tot_{events_i} - \sqrt{Tot_{events_i}}\right)$

For each co-ordinate axis the choice of detectors used in the above expressions is based on the recorded intensities.

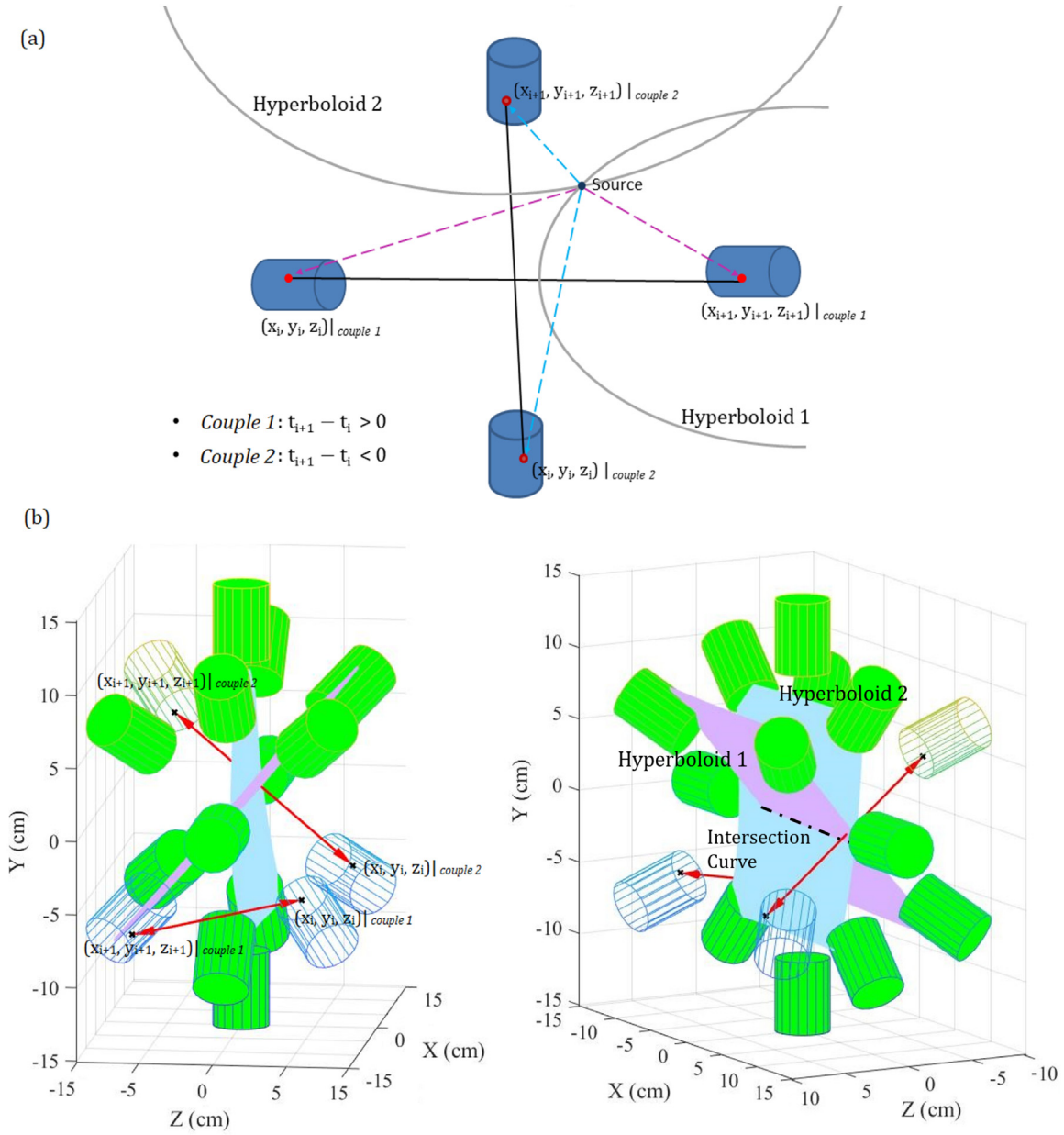

Fig. 5. (a) Schematic and (b) 3D illustration of the third function of the algorithm, Source-Position Reconstruction: the intersection between two consecutive *half*-hyperboloids is calculated. The original source position should lie somewhere on the intersection curve.

2.3.4. Function3: Source position reconstruction — analysis intersection points

Each intersection between two *half*-hyperboloids results in a series of points in the full three dimensional space. The amount of points per intersection depends on both the cube and the voxel sizes. In the third function of the algorithm a curve is obtained by fitting the points with a 3rd order polynomial function. All curves are stored, for a maximum of $n/2$ curves. For each couple of curves the intersection-point is determined. When all intersections are non-null a maximum number of $2 \cdot (n/2) = n$ intersection points, i.e. possible source positions, are found.

Small uncertainties may affect the parameters of the hyperboloids. These uncertainties are reflected in the intersection calculation. New uncertainties are also introduced by the use of the polynomial fit. As a result the curves may not cross each other. To overcome this, for each couple of curves C_1 and C_2, the following analysis is performed:

1. The points $P_1 = (x_{c_1}, y_{c_1}, z_{c_1})$ and $P_2 = (x_{c_2}, y_{c_2}, z_{c_2})$, belonging to C_1 and C_2 respectively, and characterised by the minimum Euclidean distance $| P_1 - P_2 |$, are selected.
2. The mean value between P_1 and P_2 is saved. It represents a virtual source position $P_{s\_p} = (x_{s\_p}, y_{s\_p}, z_{s\_p})$:

$$x_{s\_p} = \frac{x_{c_1} + x_{c_2}}{2} \quad y_{s\_p} = \frac{y_{c_1} + y_{c_2}}{2} \quad z_{s\_p} = \frac{z_{c_1} + z_{c_2}}{2}.$$

All the virtual source positions are saved. They represent the reconstructed coordinates in which the source was located and, as such, they are the final outcome of the algorithm.

2.4. Geant4 evaluation

The Geant4 Monte-Carlo Toolkit (version 10.04) [15] has been employed to simulate the spectrometer and an isotropic ^{60}Co source at various known locations within the spectrometer's central area. To facilitate swift simulation and reconstruction time

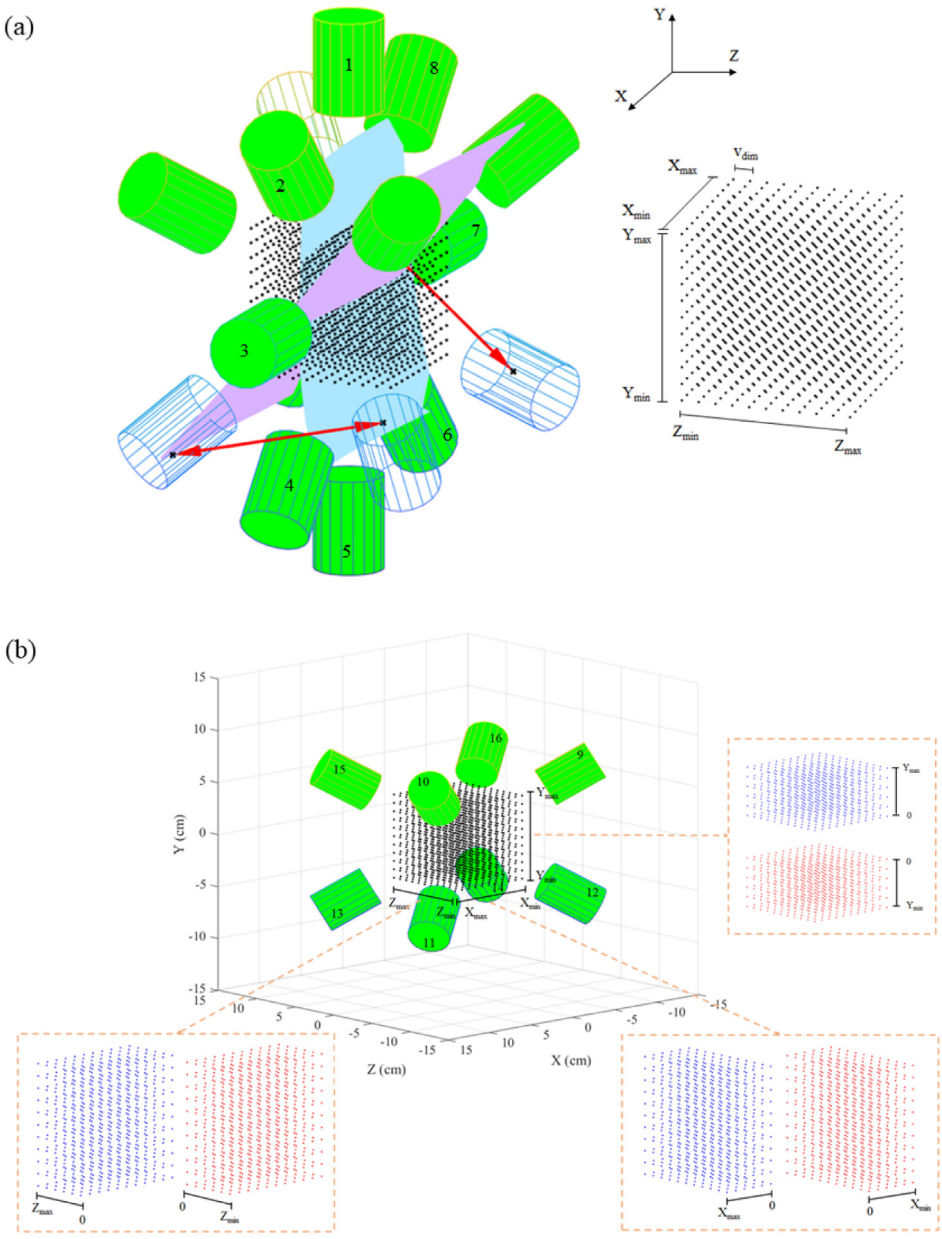

Fig. 6. (a) In the third function of the algorithm, Source-Position Reconstruction, the intersection between two triangulated *half*-hyperboloids is calculated. Each intersection is estimated inside a virtual voxelated cube located in the central area of the spectrometer. If two *half*-hyperboloids intersect into a specific voxel, the central point of the voxel is saved as an intersection point. Consequently, for each couple of intersecting *half*-hyperboloids, a sequence of points along the intersection 3D curve are produced. The larger the dimensions of the voxelised cube are (X_{neg}/X_{pos}, Y_{neg}/Y_{pos}, Z_{neg}/Z_{pos}) the wider the sampled area is. By increasing the cube dimensions, the algorithm computational time extends. (b) The cube dimensions can be reduced along the three axes independently by employing the intensity of the γ-rays recorded in the detectors at backward/forward angles. The computational time is then shortened.

the internal radius of the spectrometer has been set to 9 cm. For the $LaBr_3$(Ce) detectors an energy resolution of 3% FWHM [12] and a time resolution of 280 ps [16] have been used. As mentioned previously the $LaBr_3$(Ce) internal activity does not impact the reconstruction process, therefore, it has not been modelled. Simulations have been performed in air with 10^5 primary events. Both electromagnetic *EmStandardPhysics4* and radioactive decay *G4DecayPhysics* physics lists have been combined together and a secondary particle production "cut" value of 0.5 mm was set to optimise run time without adversely affecting precision. The ^{60}Co γ-rays are detected and recorded by the virtual spectrometer.

When a γ-ray enters the sensitive area of a detector it can Compton scatter multiple times, termed *hits*, prior to absorption via the photoelectric effect. For every γ_i ray detected several pieces of information are registered (see Fig. 7):

1. Det_i = the detector number in which γ_i has been registered;
2. E_i = the total energy by γ_i in Det_i deposited (sum of the energy deposited in all hits in Det_i);
3. t_i = the emission and arrival time difference of γ_i in Det_i.

As the γ-ray emission time is available in the Geant4 simulation this is utilised to calculate the relative arrival times of the detected γ-ray couple. This serves the same purpose as an electronic event time stamp module used in a real spectroscopy applications. The detector outputs are then passed to the algorithm which reconstructs the 3D coordinate of the ^{60}Co source.

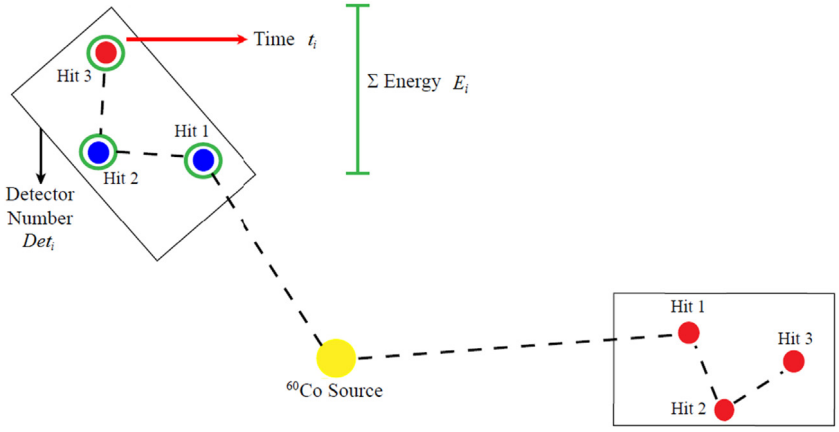

Fig. 7. During a simulation, for every ^{60}Co-emitted γ-ray γ_i recorded in a detector, several pieces of information are saved: the detector number Det_i, the total energy released E_i, and the time t_i of the last hit.

2.5. Hit positions values identification

For each γ-ray recorded by the spectrometer the algorithm is fed the coordinates of the last hit position within the detector medium. Monte-Carlo simulations provide these coordinates exactly, however, as with many large crystal, non position sensitive detectors, this information is not available in reality. In order to obtain an accurate estimate of the final interaction position for a real detector, the Geant4 simulation was used to obtain a 3D probably distribution of photoelectric γ-ray interactions. For this 10^8 ^{60}Co decays were modelled for a source located at (0,0,0). From this data Probability Density Functions (PDFs) for each dimension are derived separately for each detector.

To closer replicate reality, in the algorithm, for each γ_i ray belonging to a *couple*, the exact coordinates of the last hit position are not employed. Conversely, once the detector Det_i in which γ_i has been absorbed is determined, the three PDFs, one for dimension, associated to Det_i, are loaded. These PDFs are sampled using the acceptance–rejection method [17] to obtain a final interaction position, in 3D, for γ_i. The described procedure reflects more accurately what would be observed when using real detectors.

3. Results

In Fig. 8a the reconstructed coordinates for a source modelled at (0,0,0) are reported. For each co-ordinate axis a Gaussian fit has been applied to the algorithm-reconstructed data. The peak centroid position, μ, corresponds to the source location coordinate with the standard deviation, σ, representing the position uncertainty. The reconstructed coordinate values $\mu \pm \sigma$ are: -0.3 ± 2.5, -0.4 ± 2.4, and -0.6 ± 2.5 mm along the X, Y, and Z axis, respectively. The source location has been accurately determined within a 3 mm uncertainty by the algorithm using only realistic detector signals. For this result, the virtual voxelised cube in which the *half*-hyperboloids intersections were calculated, as described in Section 2.3.3, had a volume of 512 cm^3 ($X_{pos} = 4$, $X_{neg} = -4$, $Y_{pos} = 4$, $Y_{neg} = -4$, $Z_{pos} = 4$; $Z_{neg} = -4$). The total number of recorded γ-rays was 19 576. This leads to a geometrical efficiency for the spectrometer, defined as the number of recorded γ-rays divided by the number of initial γ rays emitted by the source, of 20%. In a total computational time of 1 h and 35 min (Windows 64 with Intel Core i7-6700 @ 3.41 GHz CPU and 16 GB RAM) the algorithm selected 566 *couples* and reconstructed 20 706 virtual source positions (x_{s_p},y_{s_p},z_{s_p}).

Fig. 8b shows the reconstructed coordinates for an isotropic source located at (20,20,20) mm. The reconstructed coordinated values, $\mu \pm \sigma$, are: 20.2 ± 1.0, 20.2 ± 0.9, and 20.1 ± 1.2 mm, along the X, Y, and Z axis, respectively. For this source location the uncertainty deduced from the Gaussian fits is less than 1.5 mm. The number of γ-rays recorded was 19 345 in agreement with the expected 20% geometrical efficiency. In a total computational time of 2 min the algorithm selected 519 *couples* and reconstructed 21 945 virtual source coordinates. The cube volume, in this case, was 64 cm^3 ($X_{pos} = 4$, $X_{neg} = 0$, $Y_{pos} = 4$, $Y_{neg} = 0$, $Z_{pos} = 4$, $Z_{neg} = 0$). For both source locations a voxel size (v_{dim}) of 0.5 mm was chosen to optimise both reconstruction precision and computational time.

4. Discussion

It is clear from the Gaussian fit results shown in Fig. 8 that the reconstructed source locations are in excellent agreement with the known values. The uncertainty associated with the reconstructed position of the source at (20,20,20) mm is better than that of the source at (0,0,0). There are two steps in the algorithm in which the position of the source plays a crucial role on the reconstruction precision: (1) the selection of only one side of the two-sheeted hyperboloid in Function 2 (Section 2.3.2), (2) the selection of the size of the virtual voxelised cube in which the intersection between two *half*-hyperboloids is estimated in Function 3 (Section 2.3.3).

Every γ-ray *couple* (γ_i and γ_{i+1}) is represented by a two-sheeted hyperboloid, with the source position lying somewhere on the hyperboloid surface. To shorten the computational time and reduce the number of false reconstructed coordinates, only one side of each two-sheeted hyperboloid, a *half*-hyperboloid, can be selected. This selection, as described in Section 2.3.2, is based on the intensity difference of the recorded γ-rays in the two detectors (Det_i and Det_{i+1}) in which the events in the *couple* have been registered. A high intensity difference leads to a correct *half*-hyperboloid selection and, as expected, the intensity difference increases as the source is shifted form the centre of the spectrometer (0,0,0).

The frequency of the correct *half*-hyperboloid selection has been investigated as a function of the source position. The source position was shifted along the positive direction of the Z axis, from 0 to 10 cm, in steps of 1 cm. Shifts of 15 and 20 cm have been evaluated also with the spectrometer radius fixed at 9 cm. For each source position, γ-ray intensity as recorded by each detector (Tot_{events_j}) was determined. For all of the recorded *couples* the detector number and the time, for each individual γ ray, are employed to evaluate the following condition:

$$\begin{aligned} &(Tot_{events_j}|_{j=Det_i} < Tot_{events_j}|_{j=Det_{i+1}} \quad AND \quad t_i > t_{i+1}) \\ &\qquad\qquad OR \\ &(Tot_{events_j}|_{j=Det_i} > Tot_{events_j}|_{j=Det_{i+1}} \quad AND \quad t_i < t_{i+1}) \end{aligned} \tag{4}$$

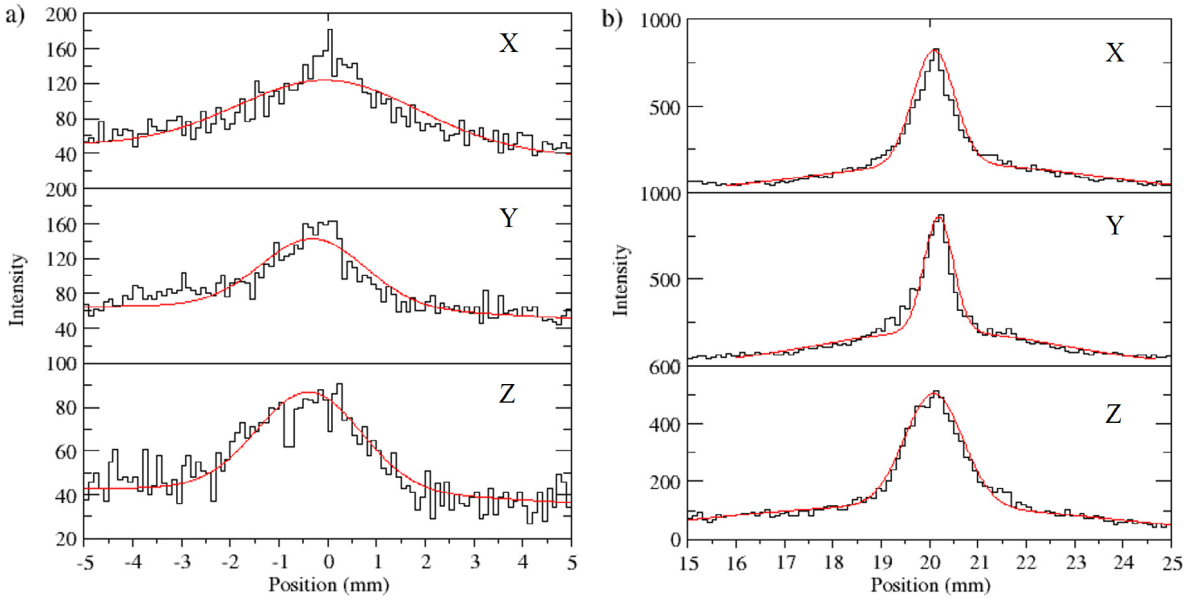

Fig. 8. Coordinates of a single isotropic ^{60}Co source simulated in (a) (0, 0, 0) and in (b) (20, 20, 20) mm as reconstructed by the in-house developed algorithm. Along each axis a Gaussian fit has been applied on the algorithm-reconstructed data. The position of the centre of the peak, μ, and the standard deviation of each peak, σ, correspond, respectively, to the reconstructed coordinate and to the uncertainty to within this coordinate is reconstructed. When the source is in (0, 0, 0) the reconstructed coordinates values ($\mu \pm \sigma$) are: -0.3 ± 2.5, -0.4 ± 2.4, and -0.6 ± 2.5 mm along the X, Y, and Z axis, respectively. When the source is in (20, 20, 20) mm the reconstruction values ($\mu \pm \sigma$) are: 20.2 ± 1.0, 20.2 ± 0.9, and 20.1 ± 1.2 mm along the X, Y, and Z axis, respectively.

If the above condition is true the time-intensity correlation holds up. Conversely if

$$\begin{aligned} &(Tot_{events_j}|_{j=Det_i} < Tot_{events_j}|_{j=Det_{i+1}} \quad AND \quad t_i < t_{i+1}) \\ &\qquad\qquad OR \\ &(Tot_{events_j}|_{j=Det_i} > Tot_{events_j}|_{j=Det_{i+1}} \quad AND \quad t_i > t_{i+1}) \end{aligned} \tag{5}$$

is upheld, there is no true time-intensity correlation (see Fig. 9). The larger the source shift from (0,0,0) the larger the fraction of *couples* that fulfil condition (4). This is observed for source locations that remain within the spectrometer radius (9 cm) as locations outside of the array result in a considerably reduced geometrical efficiency. It is imperative that for this technique to work as described the source needs to be located within the central spectrometer volume.

As explained in Section 2.3.3 each intersection between two half-hyperboloids is calculated in a virtual voxelised cube in the spectrometer central volume. The cube size can be reduced, without affecting the reconstruction precision, by using the difference between the intensities of the recorded γ-rays for the detectors at forward and backward angles (Fig. 6b). When the source is at (0,0,0) it subtends, to within statistical uncertainty, the same solid angle for all detectors. In this special case, where the source is exactly located at the centre of the spectrometer, the cube size cannot be reduced because there is no intensity difference between the forward and backward detectors. When the source is located at (20,20,20) mm the intensity difference is significant and the cube size can be reduced. The cube volume is 512 cm^3 ($8 \times 8 \times 8$ cm) and 64 cm^3 ($4 \times 4 \times 4$ cm) when the source is located at (0,0,0) and (20,20,20) mm, respectively. A large cube size, like the one needed for a centrally located source, results in a longer computational time and an increased number of false reconstruction co-ordinates compared to smaller cube sizes. Bearing this in mind a prototype spectrometer should be movable and/or have the ability to adjust the detector angles. One benefit of having a centrally located source with this type of spectrometer is that is can be used to measure absolute source activities [18].

In the current work, for both source locations, a voxel size v_{dim} of 0.5 mm was set to optimise between precision and computational time. For some applications, however, a larger value may be chosen to improve precision. An analysis concerning the dependence of the algorithm accuracy, precision, and computational cost from v_{dim} has been carried out. The simulation output, relative to a source at (0,0,0), has been passed to the algorithm and, in six different runs, v_{dim} was set to: 5, 4, 2, 1, 0.5, and 0.2 mm. It has been noticed that, by increasing v_{dim}, the algorithm computational time significantly increases, passing from $\sim$ 11 s for $v_{dim} = 5$ mm to $\sim$ 5 h 58 min for $v_{dim} = 0.2$ mm. The algorithm source reconstruction is achievable, along each axis, to within 2.5 and 4 mm, when v_{dim} is 0.2 and 5 mm, respectively.

To put the results from this work in perspective, a clinical SPECT γ-camera offers a spatial resolution for radioactive source location on the order of 4–6 mm [2]. The spatial resolution with the technique detailed above is superior for non-centrally located sources. It is clear that this technique could be successfully adapted to be used in a number of radioactive source applications including nuclear medicine and national security.

As previously mentioned this technique could also be used for distributed γ-ray sources such as those found in proton beam radiotherapy. One possible usage would be in the reduction of range uncertainty through the detection and position reconstruction of prompt-gamma (PG) rays emitted naturally during therapy. Due to the high energy of the PG-rays and to the huge neutron contamination, PG-rays detection with standard imaging instruments employed in nuclear medicine is inefficient; an optimised device needs to be designed [19]. Although, in the last decade, different detector systems have been proposed, several problems impede their clinical potential [4]. Collimated gamma cameras have been initially used to demonstrate the feasibility of PG-ray detection for range verification [3,20]. In spite of the collimation used in these systems, the signal is significantly blurred by background neutron radiation [7,21,22]. The coincidence requirement of the algorithm described above discriminates between neutron and γ radiation improving the imaging capability of the system. One of the most abundant PG-ray emitters in human tissues is ^{16}O. As opposed to a ^{60}Co source the γ-ray *couples* for the algorithm would be the 2.741 (I^{π}: $2^- \rightarrow 3^-$) and 6.128 (I^{π}: $3^- \rightarrow$ g.s.) MeV (p, ^{16}O)-induced PG-rays [23]. These de-excitations,

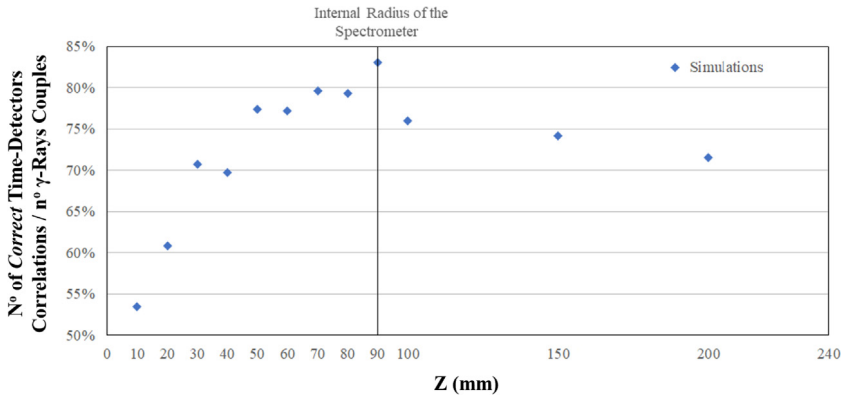

Fig. 9. Second function of the algorithm, γ-Ray Couples Analysis: the number of *correct* time-detectors correlations divided by the total number of *couples* as a function of the source shift along the positive direction of the Z axis. The internal radius of the spectrometer has always been kept at 9 cm. For a source shift shorter then 9 cm the fraction of *couples* characterised by a *correct* correlation increases with the shift magnitude. On the other hand, for shifts bigger than 9 cm the γ-rays are no more easily geometrically detectable by all the detectors and the number of *correct* correlations decreases.

from a particular ^{16}O nucleus, are effectively, within detection resolution, emitted simultaneously in position and time, almost along the entire proton beam path. The $LaBr_3(Ce)$ spectrometer coupled with the position reconstruction algorithm provides a unique system for tackling the challenge of range uncertainty in proton beam therapy. Discussions are currently being held with clinical scientist colleagues for a small design adaptation of the spectrometer to enable clinical implementation.

The simulation described in this work, with the source at (0,0,0), has been repeated varying the number of primary events: 10^3, 10^4, 10^5, and 10^6. It has been found that both accuracy and precision improve with increasing primary events. With 10^4 primary events, which translates to $\sim$ 1900 recoded γ-rays and $\sim$ 60 *couples*, the algorithm is able to reconstruct the source position with a 6 mm uncertainty, within $\sim$ 10 min on the stated system. Conversely, with 10^6 primary events, which implies $\sim$ 197 600 recoded γ-rays and $\sim$ 5800 *couples*, the source reconstruction is achieved with a 2 mm uncertainty, but at the price of a long computational time ($\sim$ 15 h). In proton beam therapy, PG rays are emitted along the beam path, effectively giving a moving γ-ray source. Initial simulation results for a 180 MeV proton beam on water show that this algorithm can reconstruct the position of the maximum intensity of the PG-rays distribution with an uncertainty of $\sim$ 4 mm for 10^8 primary proton events. Verburg et al. [7] showed hat $1.64 \cdot 10^7$ PG-rays are emitted per gram of ^{16}O per Gray of dose delivered.

Conclusions

A new method to determine the location of a radiative source, with millimetric accuracy and without knowing the radiation emission time, has been developed. The method is based on the detection of two γ-rays in coincidence. A spectrometer comprising 16 conventional $LaBr_3(Ce)$ detectors in a symmetrical configuration is employed to detect the source emitted radiation. A source position reconstruction algorithm has been developed; it takes as inputs the $LaBr_3(Ce)$ detector signals and reconstructs the position of the γ-ray source, in full three dimensional space. The algorithm only needs the signals available through standard electronics couple to off-the-shelf scintillator detectors. The spectrometer-algorithm performance has been investigated for a ^{60}Co source in two different positions within the central area of the spectrometer. The results show that for sources located at (0,0,0) and (20,20,20) mm the reconstructed location is determined with uncertainties of less than 3 mm and 2 mm, respectively. The developed method has a wide range of possible future research/industrial applications such as source localisation in nuclear medicine, security and radioactive waste assays. The system will also work for distributed sources and could aid in minimising range uncertainty in proton beam therapy. The present article is not intended as documentation for the code mentioned, instead, it describes a general methodology to generate a position reconstruction algorithm. Further developments are ongoing to improve the algorithm and to empirically validate the spectrometer-algorithm performance.

Declaration of competing interest

The authors declare that they have no known competing financial interests or personal relationships that could have appeared to influence the work reported in this paper.

CRediT authorship contribution statement

Costanza M.V. Panaino: Data curation, Formal analysis, Investigation, Methodology, Validation, Visualisation, Writing - original draft, Writing - review & editing. **Ranald I. Mackay:** Supervision, Writing - review & editing. **Marios Sotiropoulos:** Conceptualisation, Writing - review & editing. **Karen J. Kirkby:** Funding acquisition, Resources, Writing - review & editing. **Michael J. Taylor:** Conceptualisation, Funding acquisition, Investigation, Project administration, Resources, Software, Supervision, Writing - review & editing.

Acknowledgements

C.M.V.P would like to acknowledge support form CRUK via the funding to Cancer Research UK Manchester Centre: [C147/A18083] and [C147/A25254].

M.S would like to acknowledge support form Marie Curie Actions – Initial Training Networks (ITN) as an Integrating Activity Supporting Postgraduate Research with Internships in Industry and Training Excellence (SPRITE) under EC contract 317169 and the Christie Charitable Fund (registered number 1049751).

M.J.T, M.S, K.J.K and R.I.M would like to acknowledge funding from the NIHR Manchester Biomedical Research centre.

References

[1] R. Estep, T. Prettyman, G. Sheppard, Nucl. Sci. Eng. 118 (1994) 145–152, http://dx.doi.org/10.13182/NSE94-A19380.

[2] T. Peterson, L. Furenlid, Phys. Med. Biol. 56 (2011) R145, http://dx.doi.org/10.1088/0031-9155/56/17/R01.
[3] C. Min, C. Kim, M. Youn, J. Kim, Appl. Phys. Lett. 89 (2006) 183517, http://dx.doi.org/10.1063/1.2378561.
[4] A. Knopf, A. Lomax, Phys. Med. Biol. 58 (2013) R131, http://dx.doi.org/10.1088/0031-9155/58/15/R131.
[5] B. Kozlovsky, R.J. Murphy, R. Ramaty, Astrophys. J. Suppl. Ser. 141 (2002) 523.
[6] C. Min, H. Lee, C. Kim, S. Lee, Med. Phys. 39 (2012) 2100–2107, http://dx.doi.org/10.1118/1.3694098.
[7] J. Verburg, K. Riley, T. Bortfeld, J. Seco, Phys. Med. Biol. 58 (2013) L37, http://dx.doi.org/10.1088/0031-9155/58/20/L37.
[8] M. Nikl, Meas. Sci. Technol. 17 (2006) R37, http://dx.doi.org/10.1088/0957-0233/17/4/R01.
[9] M. Bé, V. Chisté, C. Dulieu, E. Browne, V. Chechev, et al., BIPM (2004).
[10] N. Schramm, G. Ebel, U. Engeland, T. Schurrat, M. Behe, et al., IEEE Trans. Nucl. Sci. 50 (2003) 315–320, http://dx.doi.org/10.1109/TNS.2003.812437.
[11] R. Nicolini, et al., Nucl. Instrum. Methods Phys. Res. A 582 (2007) 554–561, http://dx.doi.org/10.1016/j.nima.2007.08.221.
[12] F. Quarati, et al., Nucl. Instrum. Methods Phys. Res. A 574 (2007) 115–120, http://dx.doi.org/10.1016/j.nima.2007.01.161.
[13] J. Harris, H. Stöcker, Handbook of Mathematics and Computational Science, 1998.
[14] N. Amato, M. Goodrich, E. Ramos, Discrete Comput. Geom. 26 (2001) 245–265, http://dx.doi.org/10.1007/s00454-001-0027-x.
[15] S. Agostinelli, et al., Nucl. Instrum. Methods Phys. Res. B 506 (2003) 250–303, http://dx.doi.org/10.1016/S0168-9002(03)01368-8.
[16] S. Aldawood, et al., Front. Oncol. 5 (2015) 270, http://dx.doi.org/10.3389/fonc.2015.00270.
[17] B. Flury, SIAM Rev. 32 (1990) 474–476.
[18] G. Lorusso, R. Shearman, P. Regan, S. Judge, S. Bell, et al., Appl. Radiat. Isot. 109 (2016) 507–511, http://dx.doi.org/10.1016/j.apradiso.2015.12.050.
[19] S. Peterson, D. Robertson, J. Polf, Phys. Med. Biol. 55 (2010) 6841, http://dx.doi.org/10.1088/0031-9155/55/22/015.
[20] C. Kim, C. Min, K. Seo, J. Kim, J. Korean Phys. Soc. 50 (2007) 1510.
[21] J. Verburg, J. Seco, Phys. Med. Biol. 59 (2014) 7089, http://dx.doi.org/10.1088/0031-9155/59/23/7089.
[22] F. Roellinghoff, et al., Phys. Med. Biol. 59 (2014) 1327, http://dx.doi.org/10.1088/0031-9155/59/5/1327.
[23] D. Tilley, H. Weller, C. Cheves, Nuclear Phys. A 564 (1993) 1–183.